Citation: Molecular Therapy — Methods & Clinical Development (2015) **2,** 15047; doi:10.1038/mtm.2015.47
Official journal of the American Society of Gene & Cell Therapy All rights reserved 2329-0501/15

www.nature.com/mtm

ARTICLE

Super-resolution imaging of nuclear import of adeno-associated virus in live cells

Joseph M Kelich[1], Jiong Ma[1], Biao Dong[2], Qizhao Wang[2], Mario Chin[2], Connor M Magura[1], Weidong Xiao[2] and Weidong Yang[1]

Adeno-associated virus (AAV) has been developed as a promising human gene therapy vector. Particularly, recombinant AAV vector (rAAV) achieves its transduction of host cells by crossing at least three physiological barriers including plasma membrane, endosomal membrane, and nuclear envelope (NE). So far, the AAV transduction mechanism has not been explored thoroughly at the single viral particle level. In this study, we employed high-speed super-resolution single-point edge-excitation sub-diffraction (SPEED) microscopy to map the events of single rAAV2 particles infecting live human cells with an unprecedented spatiotemporal resolution of 9–12 nm and 2–20 ms. Data reveal that rAAV2 particles are imported through nuclear pore complexes (NPCs) rather than nuclear membrane budding into the nucleus. Moreover, approximately 17% of the rAAV2 molecules starting from the cytoplasm successfully transverse the NPCs to reach the nucleoplasm, revealing that the NPCs act as a strict selective step for AAV delivery. This study lastly suggests a new pathway to improve AAV vectors for human gene therapy.

Molecular Therapy — Methods & Clinical Development (2015) **2**, 15047; doi:10.1038/mtm.2015.47; published online 2 December 2015

INTRODUCTION

The adeno-associated virus (AAV) is a parvovirus that lacks pathogenic capabilities. It contains no viral envelope and the capsid forms an icosahedral geometry with diameters around 23 nm.[1,2] Packed inside the capsid is a linear single-stranded genome between 4–6 kb in size.[3,4] As a helper-dependent virus, AAV requires the presence of a helper virus in order to efficiently generate viral progeny. Alternatively, in the absence of coinfection with a helper virus, AAV integrates its DNA into the host cell, more specifically into 19q13.3-qter on chromosome 19 of humans.[5–10] Thus, AAV has both a lytic and lysogenic phase. Specifically, taking advantage of the lysogenic activity in the absence of coinfection, researchers have begun to utilize wild-type AAV or recombinant AAV (rAAV) in attempts to treat disease phenotypes including cytstic fibrosis,[11] hemophilia,[12] collagen-induced arthritis,[13] and more. For gene therapy, one great advantage of AAV is the capacity to infect numerous cell types including those of the nervous system,[10,14–17] lung, retina,[16] liver,[17] muscle[17] as well as endothelial cells, and more. Expression of proteins coded by rAAV vectors has also been shown to last for months following introduction of AAV to mammalian cells.[10] Despite purification methods being significantly improved in recent years, AAV-based gene therapy still faces several challenges including identifying the optimal serotype for each target cell or tissue type.[18]

AAV infection begins with endocytosis along the plasma membrane via clathrin-coated pits or by caveolae-mediated endocytosis,[19] in which AAV receptors such as sialic acids or heparin sulfate proteoglycan are utilized.[20] Subsequently, the viral particles are further sequestered into endosomes where they remain only a short time before escaping into the cytoplasm. Once freely in the cytoplasm, AAV particle can begin to translocate into the nucleus and release its genome.[19] Currently, several viral entry pathways have been reported. The viral entry pathways vary depending on the viral particle sizes, structure, and the type of host cell. Large viruses such as HIV-1 usually dissemble into pieces before their genomes and viral proteins could be delivered into the nucleus through nuclear pore complexes (NPCs) embedded on the nuclear envelope (NE).[21] In contrast, many small viruses can transport directly through the NPCs in an intact form since they are small enough to move through the NPC. Upon reaching the nucleus, the viral particles can be disassembled and the viral genome is released for transduction. Uniquely, some other viruses such as Herpesvirus can completely avoid going through the NPC by uncoating their genome at the NPC or prior to reaching the NPC. Alternatively, viruses may directly cross the NE by utilizing the temporally disassembled NE during mitosis (often used by retroviruses) or potentially through nuclear membrane budding mechanisms (by parvoviruses).[22]

In eukaryotic cells, two distinct mechanisms of nucleocytoplasmic transport through the NPC have been identified: passive diffusion and facilitated translocation. The former is reserved for signal-independent diffusing molecules that are smaller than 40 kDa (~10 nm in diameter), and the latter ensures efficient and timely translation of signal-dependent cargo molecules assisted by transport receptors (TRs) through the NPC.[23–25] Moreover, passively diffusing molecules take a transport route consistent with a size-confinement mechanism through a central axial channel.[23] On the other hand, facilitated translocation involves interactions between TRs and intrinsically

[1]Department of Biology, Temple University, Philadelphia, Pennsylvania, USA; [2]Department of Microbiology and Immunology, School of Medicine, Temple University, Philadelphia, Pennsylvania, USA. Correspondence: W Yang (weidong.yang@temple.edu) Or W Xiao (wxiao@temple.edu)
Received 24 August 2015; accepted 26 October 2015

disordered nucleoporins (Nups) rich in phenylalanine-glycine (FG) repeats. These FG-Nups comprise one third of all Nups of the NPC and together create a selectively permeable entropic barrier in arguably a form of "polymer brush" or a form of "hydrogel meshwork" for transiting macromolecules.[25–29] An AAV capsid is ~23 nm in diameter and over 5 MDa in molecular weight,[30] unlikely moving through the NPCs if not carrying nuclear localization sequences (NLSs) recognized by native TRs. In support of the notion that AAV particles cross the NE through the NPC, a recent study using rAAV serotype 2 (rAAV2) and a lectin blockade of the NPC resulted in inhibition of nuclear import.[31] Potential NLS signals also have been identified on capsid proteins of AAV2.[32–34] Moreover, rAAV2 has been shown to colocalize with the nuclear transport receptor Importin β (Imp β) and siRNA knockdown of Imp β led to partial inhibition of nuclear import and transduction of rAAV2 (ref. 31). Additionally, it is believed that different species of importins may also play roles in AAV import and different serotypes may bind different nuclear TRs. Interestingly, AAV particles have been shown accumulating in the perinuclear space of infected cells many hours after incubation. In addition, nuclear penetration of fluorescently labeled AAV2 particles has been shown to continue in the presence of several nucleocytoplasmic transport inhibitors including thapsigargin.[35] Thus contradicting data exists as to how AAV particles reach the nucleus.

Confocal fluorescence microscopy studies have shown that rAAV foci appear within the nucleus in 3 hours and progressively accumulate to reach peak concentration between 8–16 hours.[35] Single-molecule techniques, however, can provide additional information as to when AAV particles first start to reach the nucleus after introduction to cells without relying on accumulation or extraction of cells at distinct time intervals.[36] It was found that in as little as 15 minutes following cellular incubation with AAV, AAV particles could first be seen in the nucleus. Moreover, a translocation efficiency of ~13% through the plasma membrane was reported as well. Quantitative determination of the transport kinetics of AAV through the NE, however, remains largely unknown. Here, we utilize single-point edge-excitation sub-diffraction (SPEED) microscopy to track single rAAV2 particles as they cross the NE, revealing their transport kinetics and spatial pathways with an unprecedented spatiotemporal resolution of 9–12 nm and 2–20 ms.

RESULTS

Nuclear import kinetics of single rAAV2 particles across the NE in live cells

To label rAAV2 particles efficiently by fluorophores for live cell imaging, we introduced a biotin-streptavidin system into the labeling process. In detail, approximately 18 biotins were linked to each rAAV2 and each biotin provided three binding sites for three streptavidins prelabeled with three Alexa Fluor 647 dyes. Our measurements revealed that the final labeling ratio is about 36 dyes per rAAV2 molecule (Figure 1a and Supplementary Figure S1). Although a negative effect of adding multiple streptavidin labels on the AAV particle in the interactions between rAAV2 and cells could not be avoided, the majority of labeled rAAV2 particles can still effectively

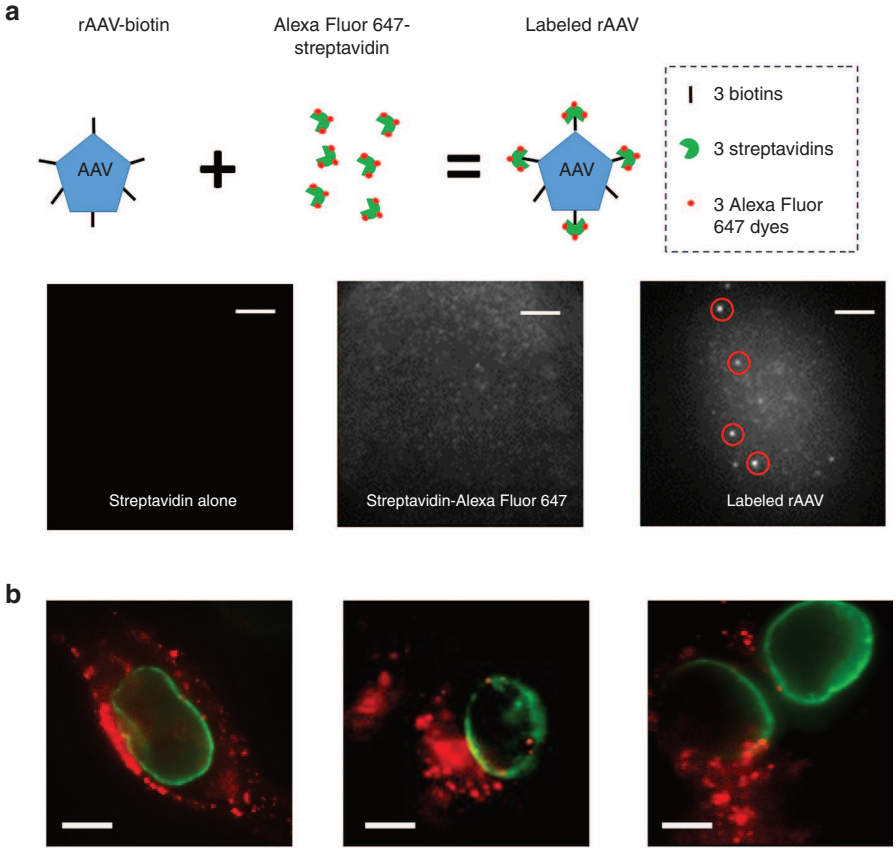

Figure 1 Labeling adeno-associated virus (AAV)2 and imaging AAV2 infection in live HeLa cells. (**a**) Up: Diagram of labeling the rAAV2-biotin with Alexa fluor 647-streptavidin; down: fluorescent image of the unlabeled streptavidin (left), labeled streptavidin (middle), and labeled rAAV2 (circled on right) at their single-molecule level. (**b**) Typical fluorescent images of labeled rAAV2 (red) infecting HeLa cells expressing Pom121-GFP (green). Some rAAV2 particles are shown in distinct isolated spots in the nucleoplasm, however most of the rAAV2 remain in the cytoplasm after incubation for 1–3 hours. Scale bar is 5 μm.

interact with host cells (Supplementary Figure S2). Beneficially, the high dye:rAAV2 labeling ratio provides high signal to noise ratio for our fluorescence microscopy imaging in bulk and at single-molecule level as shown below.

We then incubated ~10,000 labeled rAAV2 particles per live HeLa cell. In each HeLa cell, a single green fluorescence protein (GFP) was tagged to a scaffold protein POM121 in the NPC and used as an indicator showing the locations of NPCs embedded on the NE. Excited by a 488-nm excitation light of epi-fluorescence microscopy, the heavily overlapped fluorescence of GFP-NPCs indicated the location of the NE by forming a bright green ring in live cells (Figure 1b and Figure 2a,c). Subsequently, by employing a second excitation laser of 632-nm in epi-fluorescence microscopy with 500-ms exposure time, we found that rAAV2 began to accumulate around the NE after approximately 1-hour incubation with HeLa cells. At the same time, clearly some rAAV2 particles have already crossed the NE and entered the nucleus (Figure 1b). Comparably, following the same procedure, rAAV1 was found to have very minimal infection with HeLa cells (data not shown).

Next, by reducing the detection time down to 20 ms per frame in video imaging, we captured single-molecule transport events of individual Alexa-Fluor-647-labeled rAAV2 molecules as they transport across the NE in live cells (Figure 2). With a spatial localization precision of ~9 nm (Supplementary Materials and Methods), we found that once a freely diffusing cytoplasmic single rAAV2 particle was seen interacting with the NE, one of two mutually exclusive outcomes occurred. Either the labeled rAAV2 particle successfully imported into the nucleoplasm or the particle failed to import and aborted back to the cytoplasm. Examples of these successful and abortive import events are shown in Figure 2. From a total of 84 rAAV2-NE interacting events, 14 were successfully imported into the nucleus yielding an import efficiency of ~17%. We also found that these imported rAAV2 never came back to the cytoplasm after they arrived in the nucleus, suggesting a nuclear export efficiency of 0% for rAAV2 particles. Here, our observation is consistent with the data obtained from Lux *et al.*[37] in which ~90% of GFP-labeled AAV particles remained in the cytoplasm, never reaching the nucleus during their whole observation and additionally coincides with the fluorescent images seen in Figure 1 with the majority of fluorescence appearing in the cytoplasm and only small isolated spots appearing within nuclei. Besides the transport efficiency, we found that rAAV2's interacting times with the NE differ between the successful and the abortive import events as well. From the successful events, an average import time of 54 ± 20 ms was obtained, which is about half of that is obtained for the abortive events (98 ± 20 ms). Noteworthy, we found that these rAAV2 particles unlikely disassembled into pieces during the entire nuclear import process because the average intensities of the successful and the abortive import events are almost the same and none of these in-transit single-molecule fluorescent spots split into two or more spots.

Additionally, after introducing Alexa-Fluor-647-labeled rAAV2 to digitonin-permeabilized HeLa cells, no import event was observed (data not shown). This could be consistent with the notion that endogenous cellular TRs or cofactors are required to assist rAAV2s to import into the nucleus, which have been largely lost in the permeabilized cell system. To test the possibility, we further added

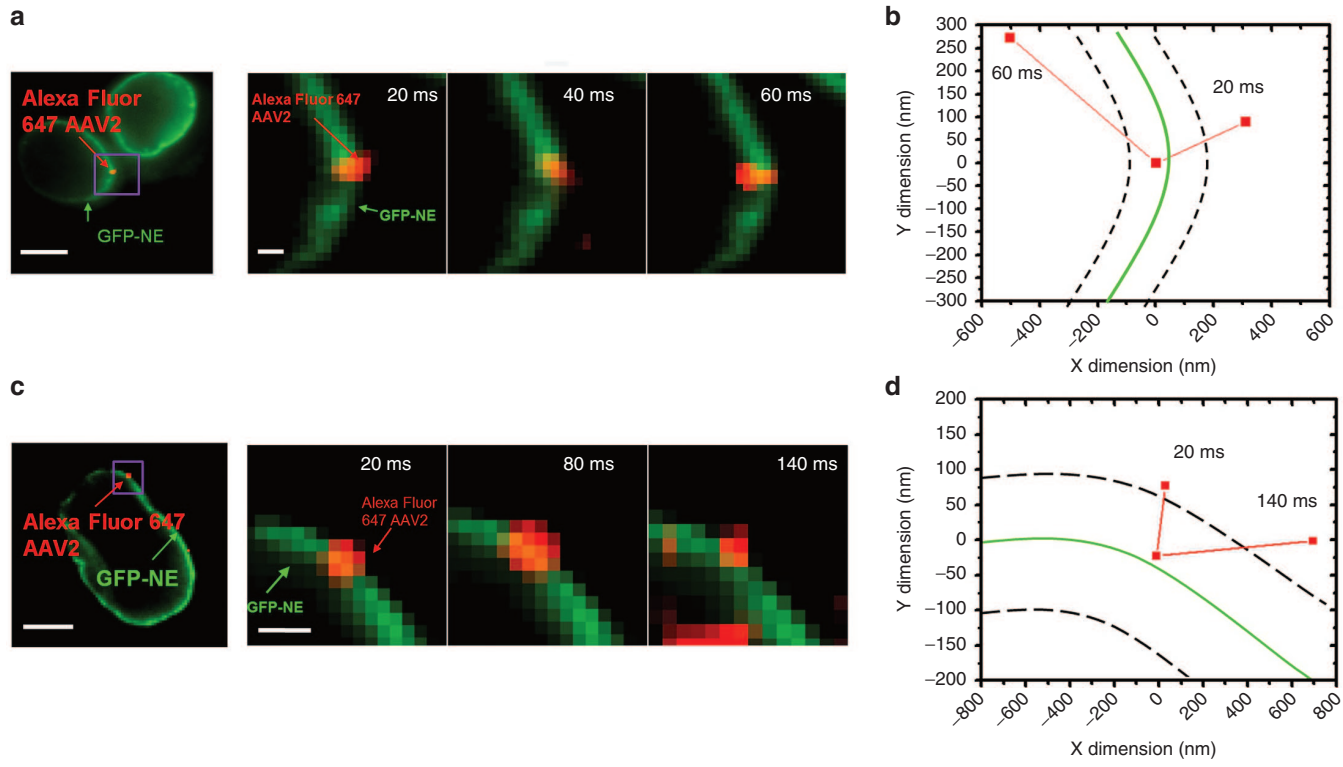

Figure 2 Single recombinant adeno-associated virus (rAAV)2 particles import into the nucleus across the nuclear envelope (NE). Single molecules are tracked as they interact with the NE region of the cell. (**a**) Typical single virus import event from the cytoplasm to the nucleoplasm after crossing the NE. A time series of images showing a successful Alexa Fluor 647-labeled rAAV2 (red) transport through the GFP-labeled NE (green). Scale bar is 5 µm for the whole cell pictures and 1 µm for the zoomed view of the import event. (**b**) The trajectory (red dots) representing the successful import event of the rAAV2 particle seen in **a**. Green line represents the middle plane of the NE, while the black dotted lines extending 100 nm on either side represent the extent of the nuclear pore complex dimension along the nucleocytoplasmic transport axis. (**c**) Images of the typical abortive rAAV2 import event. (**d**) The trajectory of the AAV2 in **c**.

0.5–1 μmol/l Imp β1 into the permeabilized cells and expected that Imp β1 could help rAA2 to import into the nucleus, but still no successful import event was observed in our measurements (data not shown). The above tests indicated that Imp β1 may not be solely responsible for or could not bind the NLSs on the transiting complexes in ferrying rAAV2 particles into the nucleus. In fact, the latter is supported by a previous report that the chemical environment of the endosome is required to expose potential NLS contained in capsid proteins of AAV particles, such as Vp1 (ref. 38).

NPCs provide a pathway for rAAV2 to import into the nucleus

To further answer the question whether rAAV2 particles enter the nucleus through the NPC or across the NE via budding, we employed SPEED microscopy to specifically examine any import events of rAAV2 through single NPCs. Technical advances in SPEED microscopy have previously enabled us to successfully track nucleocytoplasmic transport of small molecules, proteins and mRNA through single NPCs.[39] Briefly, in this work, we have utilized the following features of SPEED microscopy to track rAAV2 transiting molecules through individual NPCs: (i) An inclined illumination point spread function (~320 nm in x, y, and z dimensions), smaller than the average nearest neighboring distance between the NPCs on the NE, enabled the excitation of a single GFP-labeled NPC in each dimension (Supplementary Figure S3). Additionally, because NPCs are not homogenously distributed in the HeLa cells (approximately 3–6 pores/μm^2),[40] we choose the least densely populated region of the NE for study to enhance imaging a single NPC in the illumination volume of SPEED microscopy; (ii) The high optical density (100–500 kW/cm^2) in the small illumination volume also squeezed out a high number of photons in a short time period from a single rAAV2 particle tagged with about 36 Alexa Fluor 647 dyes. Typically, more than 3,000 photons were obtained from a single-labeled rAAV2 particle within a 2-ms detection time. To reduce any photobleaching and phototoxic effects, an optical chopper was used to create an on/off operational mode with off-time 10-fold longer than on-time; (iii) The inclined illumination volume further greatly avoided out-of-focus background fluorescence and auto-fluorescence of the objective, which enhanced a higher SNR (>11). (iv) The small illumination volume of SPEED microscopy allowed the imaging of single molecules within a small pixel area of the charge-coupled device (CCD) camera, resulting in a fast detection speed (up to 5,000 frames per second). (v) The fast detection speed greatly reduced the spatial localization error in determining the spatial trajectories of moving rAAV2 particles in live cells, which enabled us to obtain a spatial localization resolution of 9–12 nm for moving rAAV2 particles (Supplementary Materials and Methods).

By illuminating single NPCs at the equator of the cell by SPEED microscopy, we tracked single-labeled rAAV2 particles as they came to interact with the NPCs (Figure 3b). Although a very low concentration of rAAV2 molecules were seen interacting with the NE, we successfully captured some import events of rAAV2 through the NPCs after scanning hundreds of NPCs (Figure 3c). In detail, these particles originated in the cytoplasm, interacted with the NPC and successfully exited the NPC to arrive in the nucleoplasm. The average import time for these events is ~12 ms. This is about fourfold faster than that recorded from the epi-fluorescence microscopy imaging of rAAV2 crossing the NE described earlier in this article. The difference may be caused by the different detection speeds used for single-NPC experiments and wide-field NE microscopy experiments at 2 and 20 ms respectively, as suggested previously.[39] Nevertheless, we for the first time tracked single rAAV2 particles being imported into the nucleus via NPCs. Again, we found these rAAV2 particles remained intact as single fluorescent spots with almost consistent intensities inside and outside the NPCs.

DISCUSSION AND CONCLUSION

Our single-molecule imaging of the interactions between rAAV2 and human cells revealed that rAAV2 particles enter the nucleus intact through the NPC and unlikely via nuclear membrane budding or disassembly of NE or disassembled pieces of viral particles. First, we have obtained single-molecule trajectories of rAAV2 moving through the NPCs or crossing the NE, but we never witnessed membrane invaginations on the NE that could have been monitored from the GFP illuminated NE. Moreover, the moving trajectories of rAAV2 molecules as they cross the NE or move through the NPC are limited within ~200 nm, which is much smaller than the micrometer-sized membrane budding or disassembly areas. Additionally, we also determined that the translocation time of rAAV2 either across the NE or through the NPC is at millisecond levels and never reached the typical membrane budding or disassembly time range (estimated at seconds to minutes). Additionally, we never observed single-molecule fluorescent spots of rAAV particles splitting into several pieces or undergoing a significant reduction in fluorescent intensity during the entire nuclear import process. This suggests that it is unlikely these particles become disassembled prior to reaching the nucleus. Therefore, our work supports the model that the intact capsid of the AAV travels through the NPC to reach the nucleus whereupon uncoating occurs.

Next, our data suggest that the NPC poses a third rate-limiting step in the infection pathway of AAV particles besides the plasma and the endosomal membranes. Previously single-molecule studies have shown that ~13% of AAV particles interacting with the plasma membrane could successfully undergo endocytosis and enter the cell,[36] which could be considered the first rate-limiting step. Although not yet quantitatively determined, the low efficiency for endosomal escape was posed as the second selective step for AAV delivery. Here we show that ~17% of single cytoplasmic AAV particles that interact with the NPC successfully reach the nucleus indicating that NPCs are a third restrictive barrier for AAV transduction.

Challenged by the above rate-limiting steps, one desirable development for AAV derived vectors would be to improve its translocation rate into the nucleus. This will help transduction occur with less virus and can aid in expression of proteins for therapeutic purposes. Compared to the transport efficiencies of endogenous and exogenous transiting molecules through the NPCs, the nuclear import efficiency of rAAV2 (~17%) is significantly lower than those obtained for native protein TRs (~50%) and mRNA (~36%) (P value < 0.05), but is close to that of artificial quantum dots (~20%) (Table 1). Several reports suggested that additions of different numbers and/or different types of NLSs on the large cargo particles could improve the nuclear import efficiency. For example, one study utilizing a dimer of maltose binding protein genetically modified to contain NLSs to recruit two distinct TRs (Imp β1 and Imp β2) demonstrated that the nuclear import rate was much higher than only one TR involved.[41] Additionally, recently, large β-gal complexes have been shown to be effectively imported into the nucleus through the NPC when a high number of Imp β1 were recruited to their nuclear import process.[42] We suggest that AAV vector performance may be enhanced by improving the nuclear import efficiency of the AAV particle. This can be approached through engineering the AAV particle to recruit either multiple TRs or more efficient TRs to the import complex.

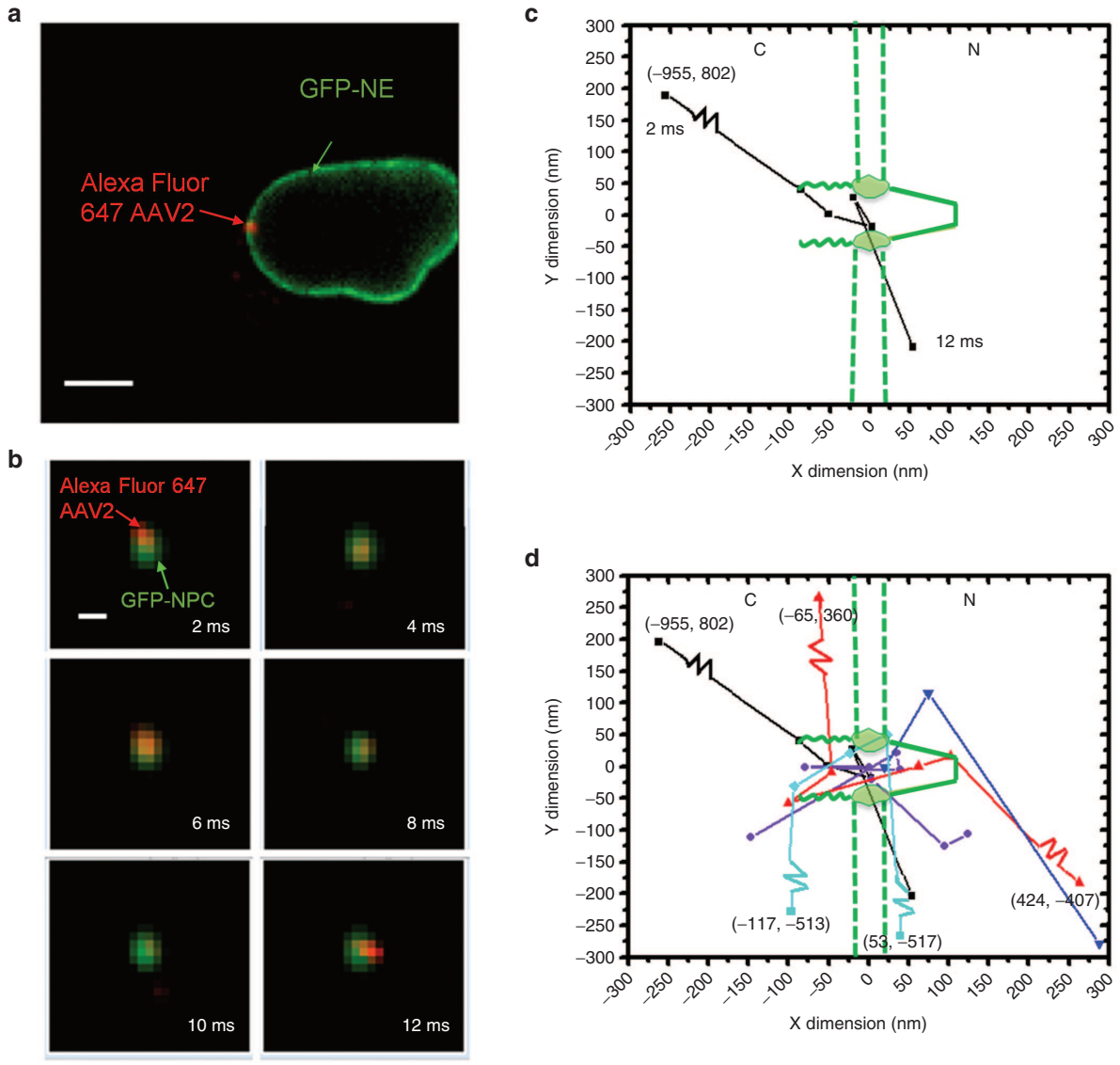

Figure 3 Single recombinant adeno-associated virus (rAAV)2 particles import into the nucleus through the nuclear pore complexes (NPCs). Single AAV2 particles are imaged and tracked importing into the nucleus through the NPC. (**a**) A single Alexa Flour 647-labeled AAV2 particle is seen interacting with the GFP-labeled nuclear envelope (NE). Scale bar: 5 µm. (**b**) A typical successful nuclear import event through the NPC for rAAV2. A single GFP-NPC is illuminated by SPEED microscopy (green). A single cytoplasmic Alexa Fluor 647-labeled rAAV2 particle is seen approaching the green NPC at 2 ms. At 4 ms, the AAV2 particle is clearly interacting with the NPC and by 12 ms it exits out the nuclear side reaching the nucleoplasm. Scale bar: 1 µm. (**c**) Plotted trajectory representing the successful nuclear import steps recorded in **b**. Even though the final plotted data point appears to cross through the NPC scaffold, we do not suggest this occurring. Instead we suggest the AAV particle crossed the NPC through the channel and moved closer to the NE after reaching the nucleoplasm. (**d**) Compiled several trajectories representing rAAV2 particles successfully importing to the nucleus from the cytoplasm through single NPCs.

MATERIALS AND METHODS

Production of AAV-biotin vector and fluorescent labeling

The DNA sequence encoding AVI peptide was inserted between 139–140 amino acid positions of VP1 in AAV2 helper plasmid, named as AVI-AAV2. A quatral plasmid cotransfection method was used to produce the rAAV2 vectors used in this study. Briefly, one vector plasmid pssAAV-CMV-LacZ, one AAV helper plasmid AVI-AAV2, one BirA-EGFP plasmid, and one mini adenovirus function helper plasmid pFΔ6, were cotransfected into HEK293 cells cultured in roller bottles at a ratio of 1:1:1:2. The transfected cells were harvested 3 days later. rAAV2 was then purified by two rounds of cesium chloride–gradient ultracentrifuge. After extensive buffer exchange against phosphate-buffered saline with 5% D-sorbitol, the peak fractions of purified virus were pooled and stored at −80 °C before administration. Alexa fluor 647-labeled streptavidin was agitated with AAV-biotin for 1 hour in 4 degree before experiment. A mixture of full/empty capsid ratio of approximately 10:1 was used for bulk and single-molecule experiments.

Cell culture and transport conditions

A HeLa cell line stably expressing the GFP-conjugate of POM121 was used, and freshly split cells were grown overnight on coverslips in Dulbecco's Modified Eagle Medium supplemented with 10% fetal bovine serum. For living cell detection, Alexa Fluor 647-labeled rAAV2 were added to the GFP-POM121 HeLa cell line with virus:cell ratio as 10,000:1. The virus and cell were incubated at 4 °C for 15 minutes. Then incubated at 37 °C for 1–3 hours.

Instrumentation

The SPEED microscope includes an Olympus IX81 equipped with a 1.4 NA 100× oil-immersion apochromatic objective (UPLSAPO 100X, Olympus, Center Valley, PA), a 35 mW 633 nm He-Ne laser (Melles Griot, Carlsbad, CA), a 120 mW ArKr tunable ion laser (Melles Griot), an on-chip multiplication gain charge-coupled device camera (Cascade 128+, Roper Scientific, Tucson, AZ) and the Slidebook software package (Intelligent Imaging Innovations,

Table 1 Transport kinetics

Molecular name	*Export efficiency (%)*	*Import efficiency (%)*	*Import/ export time (ms)*	*Detection time per frame (ms)*
rAAV2 (this paper)	~0	17 ± 4	54 ± 20	20
	N/A	N/A	12 ± 2	2
Imp β1 (ref. 47)	49 ± 5	50 ± 5	5 ± 2	2
mRNA[39]	36 ± 5	~0	11 ± 2	2
Quantum dots[48]	N/A	~20	> 2 (seconds)	25

N/A, not available; rAAV, recombinant adeno-associated virus.

Denver, CO) for data acquisition and processing. A 17-nm focal length lens was added to set an epi-fluorescent setup where the diameter of the efficient excitation region was about 12 μm. GFP and Alexa Fluor 647 fluorescence were excited by 488 and 633 nm lasers, respectively. The two lasers were combined by an optical filter (FFF555/646 Di01, Semrock, Rochester, NY), collimated and focused into an overlapped illumination volume in the focal plane. The green and red fluorescence emissions were collected by the same objective, filtered by a dichroic filter (Di01- R405/488/561/635-25x36, Semrock) and an emission filter (NF01- 405/488/561/635-25X5.0, Semrock) and imaged by an identical CCD camera.

Localization of the NE and NPC orientation

The position of the NE was determined at super-accuracy by fitting the fluorescence of GFP-POM121 as follows. The pixel intensities within a row or a column approximately perpendicular to the NE were fit with a Gaussian. The peak position of the Gaussian for a particular set of pixel intensities was considered the NE position for that row and column. The peak positions of a series of such Gaussians were then fit with a second-degree polynomial, yielding the orientation of the NE within the entire image.

The following rules were then used to select a single NPC and determine its orientation, which needs to be perpendicular to the NE on the equator of the nucleus and to the y direction of the Cartesian coordinates (x, y) in the CCD camera: (i) To focus on a GFP-NPC with eight copies of GFP-POM121, individual GFP-NPCs on the NE were selected when their fluorescence intensity was ~8-fold that of a single GFP; (ii) we chose a fluorescent NPC on the equator of the nucleus such that the tangent of the NE at the location of this NPC was parallel to the y-direction of the Cartesian coordinates (x, y) in the CCD camera; and (iii) we examined the ratio of Gaussian widths in the long and short axes of the chosen GFP-NPC fluorescence spot, which needed to fall between 1.74 and 1.82. Within this range, an illuminated NPC only has a free angle of 1.4° to the perpendicular direction to the NE.

Localization precisions of isolated fluorescent spots

The localization precision for fluorescent NPCs, immobile fluorescence molecules, and moving fluorescence molecules was defined as how precisely the central point of each detected fluorescent diffraction-limited spot was determined. For immobile molecules or fluorescent NPCs, the fluorescent spot was fitted to a 2D symmetrical or an elliptical Gaussian function, respectively, and the localization precision was determined by the standard deviation of multiple measurements of the central point. However, for moving molecules, the influence of particle motion during image acquisition should be considered in the determination of localization precision. In detail, the localization precision for moving substrates (σ) was determined by an algorithm of $\sigma = \sqrt{F(16(s^2 + a^2/12)/9N + 8\pi b^2(s^2 + a^2/12)^2/a^2N^2)}$, where F is equal to 2, N is the number of collected photons, a is the effective pixel size of the detector, b is the standard deviation of the background in photons per pixel, and $s = \sqrt{s_0^2 + 1/3D\Delta t}$, s_0 is the standard deviation of the point spread function in the focal plane, D is the diffusion coefficient of substrate in the NPC and Δt is the image acquisition time.[43–46]

In our measurements, the localization precision was 6–9 nm for moving rAAV2s according to the above equations. Due to the inevitable vibration of NPCs in the NE of living cells, the localization precision of the NPC centroid was ~6 nm. Additionally, based on the detection of 230 immobile Alexa Fluor 647-labeled GFP molecules adsorbed on a coverslip, the system error of aligned red and green fluorescence channels was determined to 3.0 ± 0.1 nm. Therefore, the overall tracking precision for rAAV2s import through the GFP-labeled NPC in living cells was estimated to ~9–12 nm.

Statistics

Experimental measurements are reported as mean ± standard error of the mean, unless otherwise noted. Binomial *Z*-test for proportions was utilized for efficiency assays.

CONFLICT OF INTEREST

The authors declare no conflict of interest.

ACKNOWLEDGMENTS

The project was supported by grants from the National Institutes of Health (NIH GM094041, GM097037, and GM116204 to W.Y.). W.X. and W.Y. designed experiments. J.M. and J.M.K. performed microscopy imaging experiments, B.D., Q.W., and M.C. purified rAAV2 particles. J.M., J.M.K., and C.M.M. performed data analysis. W.X. and W.Y. supervised the project. J.M.K, C.M.M., W.X., and W.Y. wrote the article.

REFERENCES

1. Berns, KI and Giraud, C (1996). Biology of adeno-associated virus. *Curr Top Microbiol Immunol* **218**: 1–23.
2. Atchison, RW, Casto, BC and Hammon, WM (1966). Electron microscopy of adenovirus-associated virus (AAV) in cell cultures. *Virology* **29**: 353–357.
3. Hoggan, MD, Blacklow, NR and Rowe, WP (1966). Studies of small DNA viruses found in various adenovirus preparations: physical, biological, and immunological characteristics. *Proc Natl Acad Sci USA* **55**: 1467–1474.
4. Yang, GS, Schmidt, M, Yan, Z, Lindbloom, JD, Harding, TC, Donahue, BA *et al.* (2002). Virus-mediated transduction of murine retina with adeno-associated virus: effects of viral capsid and genome size. *J Virol* **76**: 7651–7660.
5. Samulski, RJ, Zhu, X, Xiao, X, Brook, JD, Housman, DE, Epstein, N *et al.* (1991). Targeted integration of adeno-associated virus (AAV) into human chromosome 19. *EMBO J* **10**: 3941–3950.
6. Kotin, RM, Siniscalco, M, Samulski, RJ, Zhu, XD, Hunter, L, Laughlin, CA *et al.* (1990). Site-specific integration by adeno-associated virus. *Proc Natl Acad Sci USA* **87**: 2211–2215.
7. Buller, RM, Janik, JE, Sebring, ED and Rose, JA (1981). Herpes simplex virus types 1 and 2 completely help adenovirus-associated virus replication. *J Virol* **40**: 241–247.
8. Timpe, JM, Verrill, KC and Trempe, JP (2006). Effects of adeno-associated virus on adenovirus replication and gene expression during coinfection. *J Virol* **80**: 7807–7815.
9. Glauser, DL, Seyffert, M, Strasser, R, Franchini, M, Laimbacher, AS, Dresch, C *et al.* (2010). Inhibition of herpes simplex virus type 1 replication by adeno-associated virus rep proteins depends on their combined DNA-binding and ATPase/helicase activities. *J Virol* **84**: 3808–3824.
10. Kaplitt, MG, Leone, P, Samulski, RJ, Xiao, X, Pfaff, DW, O'Malley, KL *et al.* (1994). Long-term gene expression and phenotypic correction using adeno-associated virus vectors in the mammalian brain. *Nat Genet* **8**: 148–154.
11. Moss, RB, Milla, C, Colombo, J, Accurso, F, Zeitlin, PL, Clancy, JP *et al.* (2007). Repeated aerosolized AAV-CFTR for treatment of cystic fibrosis: a randomized placebo-controlled phase 2B trial. *Hum Gene Ther* **18**: 726–732.
12. Manno, CS, Chew, AJ, Hutchison, S, Larson, PJ, Herzog, RW, Arruda, VR *et al.* (2003). AAV-mediated factor IX gene transfer to skeletal muscle in patients with severe hemophilia B. *Blood* **101**: 2963–2972.
13. Cottard, V, Mulleman, D, Bouille, P, Mezzina, M, Boissier, MC and Bessis, N (2000). Adeno-associated virus-mediated delivery of IL-4 prevents collagen-induced arthritis. *Gene Ther* **7**: 1930–1939.
14. Fu, H, Muenzer, J, Samulski, RJ, Breese, G, Sifford, J, Zeng, X *et al.* (2003). Self-complementary adeno-associated virus serotype 2 vector: global distribution and broad dispersion of AAV-mediated transgene expression in mouse brain. *Mol Ther* **8**: 911–917.
15. Zhang, H, Yang, B, Mu, X, Ahmed, SS, Su, Q, He, R *et al.* (2011). Several rAAV vectors efficiently cross the blood-brain barrier and transduce neurons and astrocytes in the neonatal mouse central nervous system. *Mol Ther* **19**: 1440–1448.
16. Ali, RR, Reichel, MB, Thrasher, AJ, Levinsky, RJ, Kinnon, C, Kanuga, N *et al.* (1996). Gene transfer into the mouse retina mediated by an adeno-associated viral vector. *Hum Mol Genet* **5**: 591–594.
17. Wang, Z, Ma, HI, Li, J, Sun, L, Zhang, J and Xiao, X (2003). Rapid and highly efficient transduction by double-stranded adeno-associated virus vectors *in vitro* and in vivo. *Gene Ther* **10**: 2105–2111.

18. Aschauer, DF, Kreuz, S and Rumpel, S (2013). Analysis of transduction efficiency, tropism and axonal transport of AAV serotypes 1, 2, 5, 6, 8 and 9 in the mouse brain. *PLoS ONE* **8**: e76310.
19. Bartlett, JS, Wilcher, R and Samulski, RJ (2000). Infectious entry pathway of adeno-associated virus and adeno-associated virus vectors. *J Virol* **74**: 2777–2785.
20. Schmidt, M, Voutetakis, A, Afione, S, Zheng, C, Mandikian, D and Chiorini, JA (2008). Adeno-associated virus type 12 (AAV12): a novel AAV serotype with sialic acid- and heparan sulfate proteoglycan-independent transduction activity. *J Virol* **82**: 1399–1406.
21. Cohen, S, Au, S and Panté, N (2011). How viruses access the nucleus. *Biochim Biophys Acta* **1813**: 1634–1645.
22. Whittaker, GR (2003). Virus nuclear import. *Adv Drug Deliv Rev* **55**: 733–747.
23. Yang, W (2013). Distinct, but not completely separate spatial transport routes in the nuclear pore complex. *Nucleus* **4**: 166–175.
24. Terry, LJ, Shows, EB and Wente, SR (2007). Crossing the nuclear envelope: hierarchical regulation of nucleocytoplasmic transport. *Science* **318**: 1412–1416.
25. Naim, B, Brumfeld, V, Kapon, R, Kiss, V, Nevo, R and Reich, Z (2007). Passive and facilitated transport in nuclear pore complexes is largely uncoupled. *J Biol Chem* **282**: 3881–3888.
26. Patel, SS, Belmont, BJ, Sante, JM and Rexach, MF (2007). Natively unfolded nucleoporins gate protein diffusion across the nuclear pore complex. *Cell* **129**: 83–96.
27. Labokha, AA, Gradmann, S, Frey, S, Hülsmann, BB, Urlaub, H, Baldus, M *et al.* (2013). Systematic analysis of barrier-forming FG hydrogels from Xenopus nuclear pore complexes. *EMBO J* **32**: 204–218.
28. Hülsmann, BB, Labokha, AA and Görlich, D (2012). The permeability of reconstituted nuclear pores provides direct evidence for the selective phase model. *Cell* **150**: 738–751.
29. Wälde, S and Kehlenbach, RH (2010). The Part and the Whole: functions of nucleoporins in nucleocytoplasmic transport. *Trends Cell Biol* **20**: 461–469.
30. Laurence, J and Franklin, M (2014). Translating gene therapy to the clinic: techniques and approaches. *Acad Press* **4**: 44–48.
31. Nicolson, SC and Samulski, RJ (2014). Recombinant adeno-associated virus utilizes host cell nuclear import machinery to enter the nucleus. *J Virol* **88**: 4132–4144.
32. Sonntag, F, Schmidt, K and Kleinschmidt, JA (2010). A viral assembly factor promotes AAV2 capsid formation in the nucleolus. *Proc Natl Acad Sci USA* **107**: 10220–10225.
33. Grieger, JC, Snowdy, S and Samulski, RJ (2006). Separate basic region motifs within the adeno-associated virus capsid proteins are essential for infectivity and assembly. *J Virol* **80**: 5199–5210.
34. Douar, AM, Poulard, K and Danos, O (2003). Deleterious effect of peptide insertions in a permissive site of the AAV2 capsid. *Virology* **309**: 203–208.
35. Cervelli, T, Palacios, JA, Zentilin, L, Mano, M, Schwartz, RA, Weitzman, MD *et al.* (2008). Processing of recombinant AAV genomes occurs in specific nuclear structures that overlap with foci of DNA-damage-response proteins. *J Cell Sci* **121**: 349–357.
36. Seisenberger, G, Ried, MU, Endress, T, Büning, H, Hallek, M and Bräuchle, C (2001). Real-time single-molecule imaging of the infection pathway of an adeno-associated virus. *Science* **294**: 1929–1932.
37. Lux, K, Goerlitz, N, Schlemminger, S, Perabo, L, Goldnau, D, Endell, J *et al.* (2005). Green fluorescent protein-tagged adeno-associated virus particles allow the study of cytosolic and nuclear trafficking. *J Virol* **79**: 11776–11787.
38. Johnson, JS, Li, C, DiPrimio, N, Weinberg, MS, McCown, TJ and Samulski, RJ (2010). Mutagenesis of adeno-associated virus type 2 capsid protein VP1 uncovers new roles for basic amino acids in trafficking and cell-specific transduction. *J Virol* **84**: 8888–8902.
39. Kelich, JM and Yang, W (2014). High-resolution imaging reveals new features of nuclear export of mRNA through the nuclear pore complexes. *Int J Mol Sci* **15**: 14492–14504.
40. Daigle, N, Beaudouin, J, Hartnell, L, Imreh, G, Hallberg, E, Lippincott-Schwartz, J *et al.* (2001). Nuclear pore complexes form immobile networks and have a very low turnover in live mammalian cells. *J Cell Biol* **154**: 71–84.
41. Ribbeck, K and Görlich, D (2002). The permeability barrier of nuclear pore complexes appears to operate via hydrophobic exclusion. *EMBO J* **21**: 2664–2671.
42. Tu, LC, Fu, G, Zilman, A and Musser, SM (2013). Large cargo transport by nuclear pores: implications for the spatial organization of FG-nucleoporins. *EMBO J* **32**: 3220–3230.
43. Mortensen, KI, Churchman, LS, Spudich, JA and Flyvbjerg, H (2010). Optimized localization analysis for single-molecule tracking and super-resolution microscopy. *Nat Methods* **7**: 377–381.
44. Quan, T, Zeng, S and Huang, ZL (2010). Localization capability and limitation of electron-multiplying charge-coupled, scientific complementary metal-oxide semiconductor, and charge-coupled devices for superresolution imaging. *J Biomed Opt* **15**: 066005.
45. Robbins, MS and Hadwen, BJ (2003). The noise performance of electron multiplying charge-coupled devices. *IEEE Trans Electron Devices* **50**: 1227–1232.
46. Deschout, H, Neyts, K and Braeckmans, K (2012). The influence of movement on the localization precision of sub-resolution particles in fluorescence microscopy. *J Biophotonics* **5**: 97–109.
47. Ma, J and Yang, W (2010). Three-dimensional distribution of transient interactions in the nuclear pore complex obtained from single-molecule snapshots. *Proc Natl Acad Sci USA* **107**: 7305–7310.
48. Lowe, AR, Siegel, JJ, Kalab, P, Siu, M, Weis, K and Liphardt, JT (2010). Selectivity mechanism of the nuclear pore complex characterized by single cargo tracking. *Nature* **467**: 600–603.

This work is licensed under a Creative Commons Attribution-NonCommercial-ShareAlike 4.0 International License. The images or other third party material in this article are included in the article's Creative Commons license, unless indicated otherwise in the credit line; if the material is not included under the Creative Commons license, users will need to obtain permission from the license holder to reproduce the material. To view a copy of this license, visit http://creativecommons.org/licenses/by-nc-sa/4.0/

Supplementary Information accompanies this paper on the *Molecular Therapy—Methods & Clinical Development* website (http://www.nature.com/mtm)